Sharing of Strain Between Nanofiber Forests and Liquid Crystals Leads to Programmable Responses to Electric Fields

Sangchul Roh, John Kim, Divya Varadharajan, Joerg Lahann, and Nicholas L. Abbott**

Fibers embedded in soft matrices are widely encountered in biological systems, with the fibers providing mechanical reinforcement or encoding of instructions for shape changes. Here, the mechanical coupling of end-attached polymeric nanofiber forests and liquid crystals (LCs) is explored, where the nanofibers are templated into prescribed shapes by the chemical vapor polymerization of paracyclophane-based monomers in supported films of the LCs. It is shown that the elastic energies of the nanofibers and LCs are comparable in magnitude, leading to reversible straining of nanofibers via the application of an electric field to the LC. This coupling is shown to encode complex electrooptical responses in the LC (e.g., optical vortices), thus illustrating how LC-templated nanofiber forests offer the basis of fresh approaches for programming configurational changes in soft materials.

1. Introduction

Fibers embedded in complex soft matrices play an essential role in shape-encoded actuation in biological systems, enabling a range of functions such as cytoskeletal control of cell shape.[1–3] In synthetic systems, prior studies have reported composites formed from fibers dispersed in isotropic matrices, but the mechanical coupling of soft nanofibers with anisotropic matrices such as liquid crystals (LCs) has not been widely explored.[1,2,4,5] Motivated by the observation that soft biological assemblies (e.g., vesicles, red blood cells, and bacterial cells), when dispersed in LCs, can be stretched or folded by the elasticity of LCs,[6–10] in this paper, we synthesize end-attached polymeric nanofibers (diameters of ≈100 nm and lengths of ≈20 μm, i.e., nanofiber forests (NFFs)) that are embedded in micrometer-thick LC films, and explore if the nanofibers are sufficiently soft that they can be strained by the elasticity of the LC.

Past studies have reported on interconnected 3D networks of nanofibers in LCs (e.g., formed by hydrogen-bond self-assembly or electrospinning) but the network structures, once formed, have not been reported to dynamically reorganize with reorientation of the LC.[11–13] Alternatively, freely suspended nanofibers in LCs have been explored (e.g., carbon nanotubes and metallic nanorods), with the nanofibers either reorienting or levitating in response to the elastic strain of the LC.[5,14–16] The nanofibers, however, were not elastically strained.[10,17,18] Herein, we report NFFs that are strained by the reorientation of LCs, and show that the strain leads to complex mechanical responses of the composite material, and the emergence of unique electrooptic responses that are programmed by the sharing of strain between the NFFs and LCs. As detailed below, the NFFs are prepared by LC-templated synthesis using chemical vapor polymerization (CVP) of [2,2] paracyclophane-based monomers.[19,20]

S. Roh, N. L. Abbott
Smith School of Chemical and Biomolecular Engineering
Cornell University
Ithaca, NY 14853, USA
E-mail: nla34@cornell.edu
J. Kim, J. Lahann
Department of Materials Science and Engineering
University of Michigan
Ann Arbor, MI 48105, USA
E-mail: lahann@umich.edu
J. Kim, J. Lahann
Biointerfaces Institute
University of Michigan
2800 Plymouth Road, Ann Arbor, MI 48109, USA
D. Varadharajan, J. Lahann
Institute of Functional Interfaces (IFG) Karlsruhe Institute of Technology (KIT) Hermann-von-Helmholtz-Platz 1
76344 Eggenstein-Leopoldshafen, Germany

2. Results and Discussion

To synthesize the NFFs used in our study, we prepared a supported LC film from 65 mol% 4-(*trans*-4-pentylcyclohexyl) benzonitrile (PCH5) and 35 mol% 4-(*trans*-4-propylcyclohexyl) benzonitrile (PCH3). The film of LC, which was confined in a copper TEM grid (transmission electron microscopy grid individual square grid size: ≈285 × 285 μm, thickness: ≈18 μm), was supported on a glass substrate coated with homeotropic polyimide (H-PI) to anchor the LC in a perpendicular (homeotropic) orientation. To load the LC into the TEM grid, ≈0.2 μL of LC was deposited into the copper TEM grid using a micropipette and excess LC was removed from the grid using a capillary tube. We used the LC film as a template for the synthesis of bent nanofibers by CVP (**Figure 1**a) using hydroxymethyl [2,2] paracyclophane (PCP-HM) as the monomer (Figure 1b). In contrast to 5CB (4-cyano-4′-pentylbiphenyl) and other nematic LCs used previously to template the growth of NFFs by CVP,[19] all of which assume perpendicular orientations (homeotropic anchoring) at the LC–air interface, PCH-based LCs adopt a horizontal orientation (planar anchoring) at interfaces to air.[21] Prior to CVP, when viewed under crossed polars, the PCH films exhibited an optical

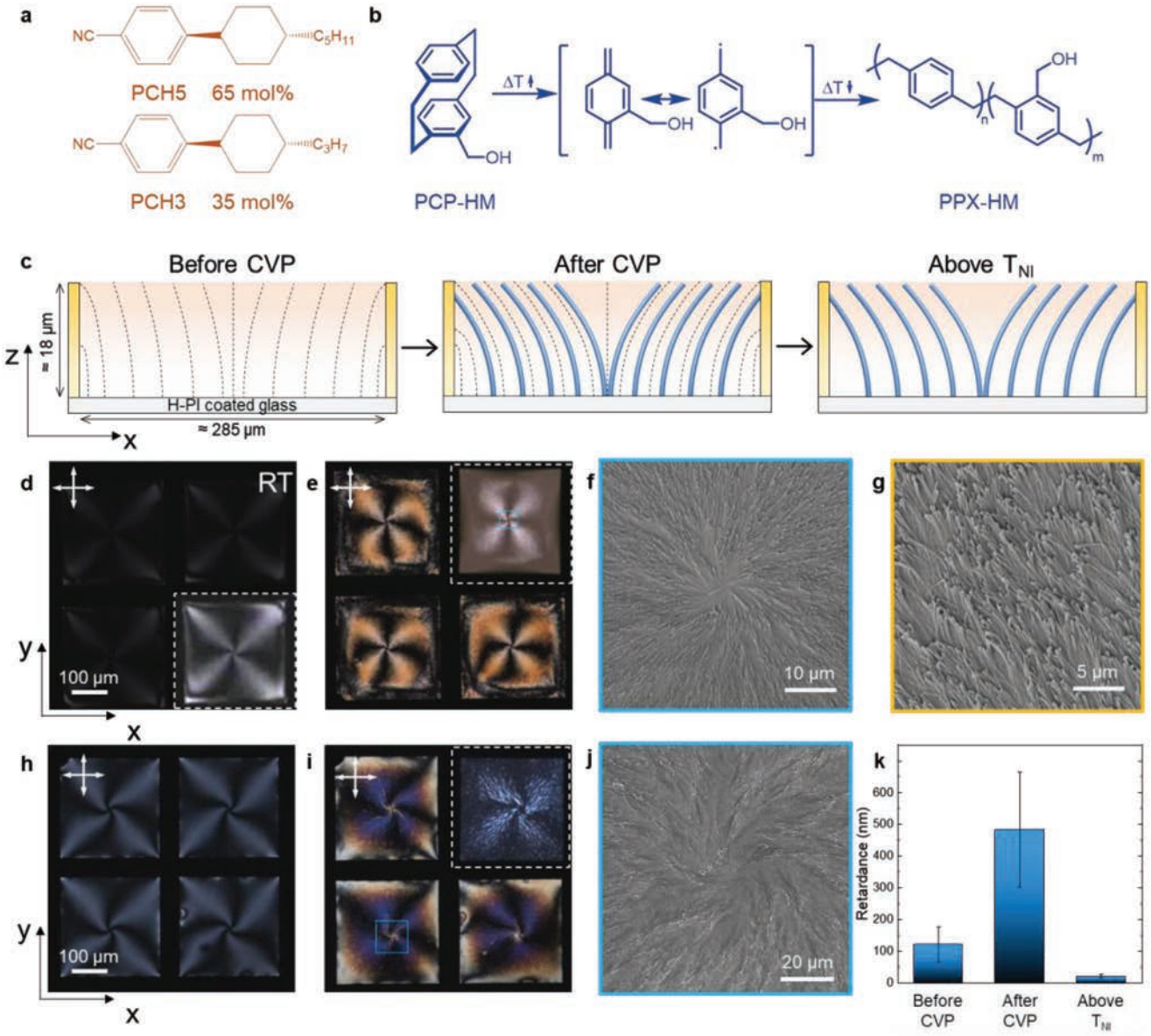

Figure 1. Synthesis of bent nanofiber forests in a LC film (PCH) using CVP. a) Molecular structures of 4-(trans-4-pentylcyclohexyl) benzonitrile (PCH5) and 4-(trans-4-propylcyclohexyl) benzonitrile (PCH3). b) A scheme showing the Gorham reaction of hydroxymethyl [2,2] paracyclophane (PCP-HM) monomers. c) Schematic illustrations of side-views of director profiles of LC and nanofibers before/after CVP and above T_{NI} (≈55 °C). Optical micrographs (crossed polarizers) of PCH LCs in individual TEM grid squares d,h) before CVP and e,i) after CVP. The insets shown in (e,i) were taken above T_{NI} (using an illumination intensity that was higher than d,e,h,i). f,g,j) Scanning electron micrographs of a nanofiber forest after removal of the PCH phase. f,j) were taken in the locations marked with a blue box in e,i), respectively. Panels (d–g) are representative micrographs of radial configurations and panels (h–j) correspond to spiral configurations, respectively. The brightness and contrast of the image shown in the bottom right corner of (d) was modified using ImageJ for clearer visualization of the birefringent pattern. The orientations of crossed polarizers are indicated in the top-left corners of each micrograph. k) Retardance changes of LC film before and after CVP and above T_{NI} of PCH (error bars: 1 SD of n = 28–48).

appearance characterized by four extinction bands (dark area in Figure 1d). The extinction bands of the PCH film correspond to regions of the film where the azimuthal orientation of the LC director is parallel to one of the crossed polarizers. In general, we observed two distinct types of extinction bands: 1) extinction bands aligned along the polarizers (≈42% of all samples prepared, Figure 1d), revealing that the LC confined within the copper grid assumes nearly a radial configuration (when viewed from above) and 2) extinction bands that are rotated from the polarizers (≈27% of all samples prepared), revealing that the LC assumes a spiral configuration (Figure 1h, see below for additional details). In both cases, the configurations adopted by the LC reflect the perpendicular anchoring of the LC on the vertical walls of the TEM grid. We found that the variation in the extinction bands (radial versus spiral) arises from changes in the curvature of the LC film surface. The LC meniscus associated with underfilling of the grid (with a radius of curvature of 2 ± 1 mm) leads to the radial configuration; overfilling (with

radius of curvature of 17 ± 10 mm) leads to the spiral configuration. The remainder of samples prepared did not exhibit well-defined patterns of extinction bands, likely due to variation in the anchoring of the LC on the vertical surfaces of the metal grids. In all samples, we measured the optical retardance, r, of the LC films to be 121 ± 56 nm (where $r = \Delta n\, d$, where Δn is the tilt angle-dependent birefringence, (Δn_{max} is ≈0.12 for the PCH mixture),[22] and d is the thickness of the LC film, ≈18 μm) (Figure 1i,k). Since PCH assumes a vertical orientation ($\theta_{z=0} = 0°$) on the H-PI-coated substrate, we used the retardance measured to calculate the orientation of the PCH at the LC-air interface to be $\theta_{z=d} = 25 \pm 7°$ (Figure 1c and Equation S1, Supporting Information for $\theta_{z=d}$ estimation). Because the easy axis of PCH is known to be horizontal (planar anchoring, $\theta_d = 90°$) at air interfaces,[21] our observation of a tilted orientation of the LC at the air interface ($\theta_d = 25 \pm 7°$) indicates that the anchoring energy of PCH at the air interface is weak compared to the H-PI (see Equation S2, Supporting Information).[16,23]

Next, we polymerized PCP-HM in a custom-built CVP reactor (Figure 1b). PCP-HM was sublimed and homolytically cleaved into quinodimethanes at an elevated temperature and transported to a deposition chamber.[24] In the deposition chamber, the LC films were placed on a rotating stage (5°C and 10 rpm) to ensure uniform deposition of polymer across the LC samples. The quinodimethanes diffuse into the PCH film and polymerize from the surface that supports the LC film.[19] We found that CVP led to a pronounced increase in the retardance of the LC film supported on the H-PI (121 ± 56 nm to 484 ± 181 nm, as shown in Figure 1e,i,k), indicating a change in the tilt angle of the LC at the air interface from $\theta_d = 25 \pm 7°$ to 54 ± 12°. In contrast, the locations of the extinction bands were unchanged by CVP, indicating that the azimuthal organization of the LC was not perturbed by CVP (Figure 1d–e,h–i). When the PCH film was heated above the nematic to isotropic transition temperature (T_{NI} ≈55 °C), the sample exhibited residual birefringence (retardance: 19 ± 6 nm), again with extinction bands nearly identical to those exhibited by the PCH at room temperature (Figure 1e,i,k). The residual retardance of the sample provides the first hint of the formation of nanofiber forests with an in-plane organization that replicates that of the PCH.

To provide additional evidence for the formation of NFFs within the PCH film, we removed the PCH using organic solvents, and imaged the surfaces with a scanning electron microscope (SEM) (Figure 1f,g,j). We observed the presence of end-attached nanofibers with average diameters of 74 ± 17 nm and lengths of 19 ± 4 μm. When characterized by SEM over an area of ≈50 μm × 50 μm, the number density of nanofibers is uniform. (Figure S1, Supporting Information). However, we do not have evidence that the nanofibers show a lateral, periodic ordering on the surface. The diameters of the nanofibers are determined by the extrapolation length of the LC (K/W ≈100 nm, where K is the LC elastic constant and W is the anchoring energy of the LC on the surface of the nanofiber).[19] The lengths of the nanofibers are comparable to the thickness of the LC film (TEM grid thickness ≈18 μm), consistent with a mechanism of templated fiber growth.[19] In addition, for the samples shown in Figure 1d,e, by comparing the NFF organization in the SEM to an optical micrograph (crossed polarizers) of the PCH LC at the same location (prior to extraction of the LC; indicated with a blue box in Figure 1e,f), we observed that the nanofibers were oriented parallel to the local orientation of the LC. This result also suggests that the LC anchors parallel to the surface of the nanofibers, which is consistent with our prior work (Figure 1d–g).[19] Overall, the results above support our conclusion that the in-plane orientation of the nematic PCH film templates the in-plane (x–y) organization of the forest of nanofibers that forms during CVP. Below, we provide additional discussion of the LC and NFF coupling observed in the samples with spiral-like extinction bands (Figure 1h–j).

The increase in optical retardance (121 ± 56 nm to 484 ± 181 nm) accompanying CVP, as noted above, also reveals that the PCH template undergoes a substantial reorganization (tilting along the z-axis) during synthesis of the NFF. This reorientation of the LC during CVP is consistent with a weakening of the anchoring energy density of the LC at the H-PI surface (w_0) caused by the growth of polymer from the H-PI surface. Specifically, for the geometry of our experiments, prior studies[16] predict that the tilt angle of the LC (θ_d) should increase with a decrease in w_0, where w_0 is the anchoring energy density at the H-PI surface (see also Equation S3, Supporting Information). Overall, we conclude that the interplay of LC elasticity and anchoring strength induces a substantial change in the configuration of the PCH template during the growth of the nanofibers. This result, more broadly, hints at the opportunity to change the LC configuration during CVP growth to program nanofiber shape.

Next, we investigated whether the presence of a NFF with a LC film changed the response of the LC film to interactions at confining surfaces. In the absence of a NFF, a PCH film (thickness: ≈32 μm) confined between two H-PI-coated substrates was observed to exhibit a dark optical appearance between crossed polars (optical retardance < 1 nm) (Figure S2, Supporting Information). To explore the influence of the NFF on the orientation of a LC film with the same confining surfaces, we prepared an 18 μm–thick NFF/PCH composite film using the procedures described above (retardance of 540 ± 53 nm: **Figure 2**a) and paired the film with a second H-PI-coated indium tin oxide (ITO) glass substrate to define a substrate-to-substrate separation of 32 μm. After filling the entire cavity with PCH, we observed the sample to exhibit a bright optical appearance with a retardance of 178 ± 22 nm (Figure 2b) and extinction bands originating from the center of the film (under crossed polarizers). We make two observations regarding this experiment. First, the retardance value of 178 ± 22 nm reveals that the NFF forest within the sample prevented the LC within the cavity from assuming a uniform perpendicular orientation (as observed in the absence of nanofibers). Second, the small value of the retardance (178 ± 22 nm) relative to the composite NFF/PCH film used to prepare the sample (540 ± 53 nm) suggests that a torque will be transmitted to the nanofibers by the LC elasticity, potentially leading to a decrease in the curvature of the nanofibers in the 32 μm-thick sample (Figure 2b) as compared to the as-synthesized fibers (Figure 2a).

To determine if the nanofibers are reshaped by elastic stresses transmitted from the LC film, we applied a 50 V AC electric field (1 kHz) to the film shown in Figure 2b. Upon

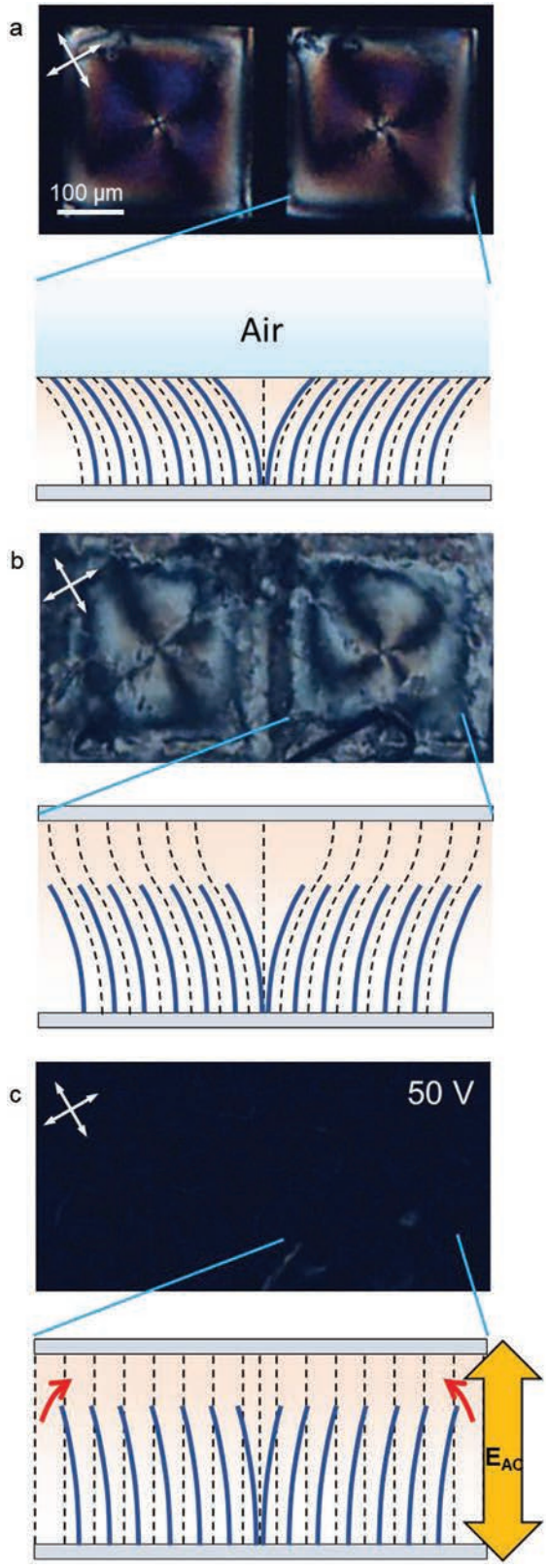

Figure 2. Optical micrographs (cross polars) of NFFs in PCH after CVP and corresponding side-view schematic illustrations. NFF and PCH composite in contact with a) air after CVP, b) H-PI-coated ITO glass, c) NFF and PCH of (b) under an electric field (50 V/1 kHz, sine wave). The orientations of the crossed polarizers are indicated in the top-left corners of each micrograph.

application of the field, we measured the retardance to decrease from 178 ± 22 nm to 5 ± 1 nm, consistent with the reorientation of the LC along the external electric field lines due to the positive dielectric anisotropy of the LC ($\Delta\varepsilon \approx 10$).[25] The change in optical retardance was reversible, with the initial configuration of the LC observed again after the removal of the external electric field. When the PCH was heated above T_{NI} in the absence of the electric field, the retardance was measured to be 8 ± 1 nm, which is larger than the retardance (5 ± 1 nm) measured under 50 V. The smaller value of the optical retardance measured with the electric field provides further evidence that the bent NFF was strained via the reorientation of the LC with the applied electric field (Figure 2c). Similar changes in the optical appearance of the PCH upon heating and application of an electric field were observed in multiple independently prepared samples (n = 12).

To obtain direct evidence of electric field-induced changes in the shapes of the end-attached nanofibers, as proposed in Figure 2b,c, we developed a procedure that allowed us to image individual nanofibers before and during the application of the electric field across the LC film. First, as described in Figure 1b,c, a network of bent NFFs was formed by CVP using a film of the PCH LC as a template (Figure 1c). Subsequently, we paired the sample with a second glass surface (surface-to-surface separation of ≈32 um), and then infused a mixture of the reactive mesogen RM257, 5CB, and 0.1 wt.% diphenyl (2,4,6-trimethylbenzoyl)phosphine oxide (TPO) (photoinitiator; **Figure 3**a,b) into the cavity between the two substrates. We then allowed the PCH, 5CB, and RM257 to mix by diffusion before photopolymerization. The glass surface induces planar anchoring of the LC mixture. Because RM257 contains two acrylate groups (Figure 3a), free-radical photopolymerization of RM257 formed a continuous 3D liquid crystalline network (Figure 3a,c) that trapped the shapes of the nanofibers.[26] Next, we detached the crosslinked composite from the substrates and immersed them into liquid nitrogen for vitrification. The vitrified LC composite was cross-sectioned with a knife, and decorated with Au/Pd by sputtering in a vacuum environment. Figure 3d shows the cross-section (15 – 20 µm from the bottom) of the composite sample prepared as described above. Significantly, we observed the tips of the nanofibers to be tilted away from the surface normal (by an angle of 31 ± 12°), consistent with the bent nanofiber geometry (Figure 3c,d). Using Equation S4 (Supporting Information), we estimated the tilt angle of the LC at z = 18 µm (height of NFF) to be ≈51°, a value that is in good agreement with the tilt angle of the LC (54 ± 12°) estimated using the LC optical retardance after CVP (Figure 1e,i,k).

Next, we explored polymerization of the NFF/LC composite films in the presence of an electric field to determine if application of the electric field to the LC strains the nanofibers. For these experiments, we followed the procedure described above using H-PI-coated ITO glass as electrodes. Prior to application of the electric field and before photopolymerization, the LC film exhibited a bright optical appearance consistent with tilting of the LC mixture containing RM257 via its interaction with the NFF (Figure S3a, Supporting Information). When an AC electric field (50 V/1 kHz) was applied across the film, we observed the film to assume a dark optical appearance (Figure S3b, Supporting Information), indicating that the LC

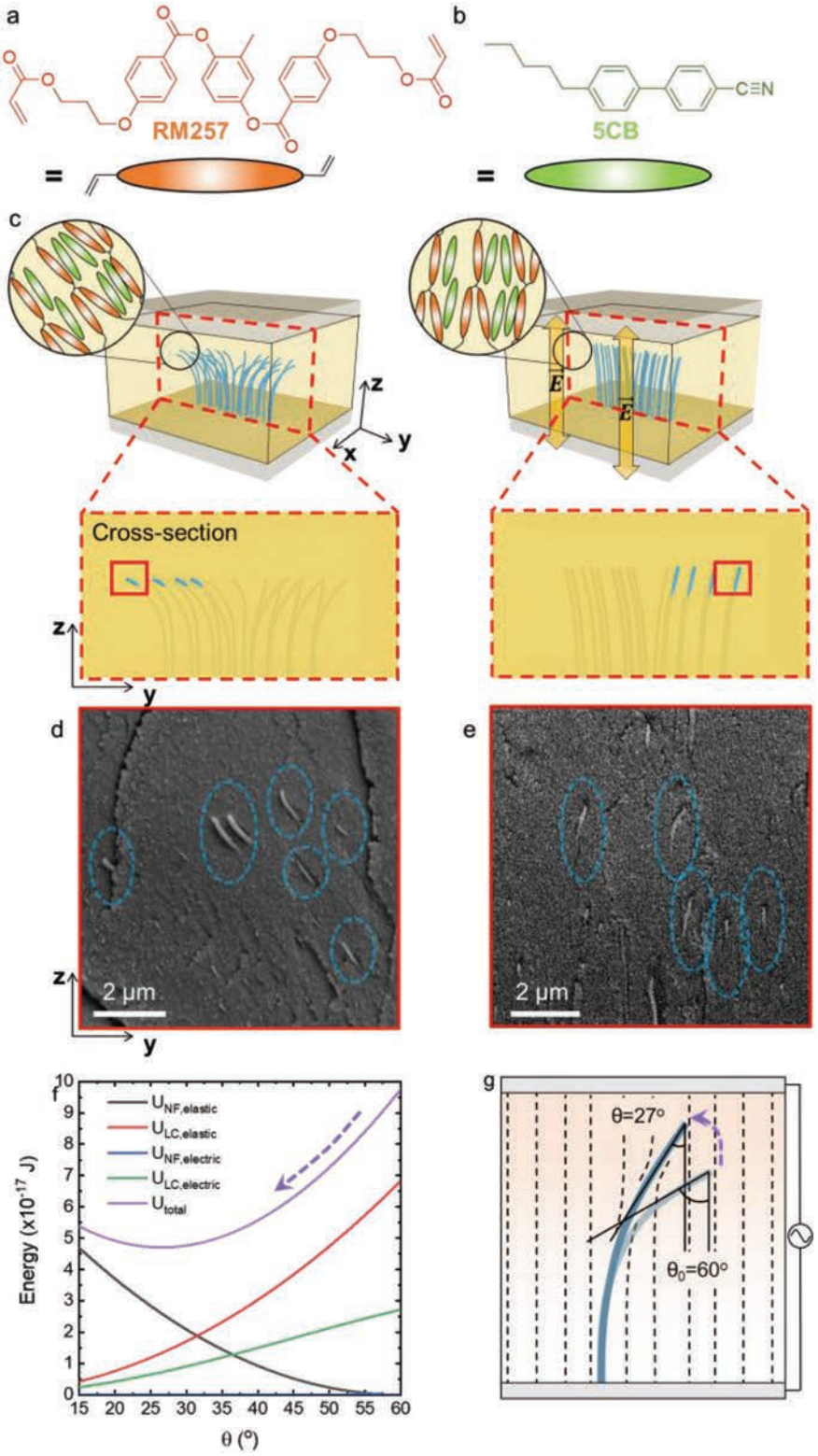

Figure 3. Molecular structures of a) polymerizable liquid crystal, RM257 (left), and b) 5CB (right). c) A schematic illustration of sample preparation for cryogenic SEM. The complete schematic of the sample preparation is also shown in the Supporting Information. Cross-sectional morphology of nanofibers embedded in crosslinked RM257/5CB prepared d) without an electric field and e) with an electric field. The blue ellipsoidal circles were intentionally added to the regions containing nanofibers. The brightness and contrast in (d–e) were adjusted using ImageJ. f) Changes in free energy stored in a nanofiber and surrounding liquid crystalline phase as a function of the tilt angle of a nanofiber (tilt angle is defined in (g). g) A schematic illustration of predicted nanofiber morphology with ($\theta = 27°$)/without ($\theta_0 = 60°$) an electric field.

composite film was aligned along the field lines (Figure 3c), an orientation that was reversed upon removal of the field (Figure S3c, Supporting Information). When the sample exposed to the electric field was polymerized by exposure to UV light, we observed the LC to exhibit a dark optical appearance both during polymerization and after removal of the electric field (Figure S3d, Supporting Information). This result suggests that the LC/nanofiber configuration induced by the electric field was preserved by the crosslinking of RM257 via free radical polymerization. When this sample was imaged by cryo-SEM, we measured the tilt angle of the nanofibers from the normal to be 6 ± 6° (Figure 3e). Because this tilt is substantially smaller than that measured in the absence of the field (31 ± 12°), we interpret this result to indicate that the nanofibers were strained along with the LC during the application of the electric field.

The results above demonstrate that the nanofibers exhibit a shape-response to the electric field, but they do not establish if the shape change was driven by the direct action of the electric field on the nanofibers or by the effect of the electric field on the LC, which in turn transmitted a mechanical torque to the nanofibers. To address this question, we developed a mechanical model for the equilibrium tilt angle of nanofibers embedded in LC by considering the free energy of the system to be composed of the elastic energy of the nanofibers ($U_{NF,elastic}$) and LC ($U_{LC,elastic}$), and the dielectric energy of the nanofibers ($U_{NF,electric}$) and LC ($U_{LC,electric}$). Our simple model assumes that the anchoring of LC on the nanofibers is strong and the orientation of LC adjacent to a nanofiber is parallel to the nanofiber (see also Supporting Information). This model predicts that a NF with an initial tilt angle of 60° decreases to 27° upon the application of 50 V (Figure 3f,g), which is a good agreement with our experimental observations (Figure 3d,e). Significantly, inspection of Figure 3f,g reveals that the nanofiber shape change is largely due to the torque imposed on the nanofiber by the LC and not due to the direct action of the field on the fiber.

The results above reveal that the elastic strain of the LC phase can reshape nanofibers grown by LC-templated CVP. The observation motivated us to explore the electrooptical properties of LCs that emerge from the sharing of strain between nanofibers and LCs. We began by optically characterizing a PCH/NFF composite with a spiral configuration (projection onto x–y plane, **Figure 4**a; see also Figure 1h–j). As noted earlier in the paper, the spiral configuration of the LC is characterized by extinction bands that are rotated from the orientations of the polarizers (Figure 1h–j). Similar to the PCH/NFF composites exhibiting the radial configuration (Figure 2), as the electric field was increased from 0 to 10 V at 1 kHz (sine wave, Figure 4a–c), the optical retardance gradually decreased (Figure 4h), consistent with the realignment of the PCH LC along the external electric field lines.

Interestingly, however, with increase in the field intensity (0 to 10 V), we observed the extinction bands to rotate (43 ± 9°) clockwise with fixed crossed polarizers (Figure 4a–c). The rotation of the extinction bands was not observed in samples with the radial configuration (Figure 2a–c). Since the extinction bands correspond to regions of the LC where the azimuthal orientation of the LC is parallel to either the polarizer or analyzer, we conclude that the LC shown in Figure 4 undergoes an azimuthal (x–y plane) reorientation in response to application of the electric field along the *z*-axis. To determine the in-plane (*x*-*y*) orientation of LC under the electric field, we inserted a first order wave plate (λ = 530 nm) when applying 10 V (Figure 4g). Yellow and cyan-blue regions indicate an in-plane orientation of LC (the *x*–*y* plane) that is parallel and perpendicular, respectively, to the slow axis of the waveplate (indicated by a blue arrow in Figure 4g). Our observation of the gradual rotation of the extinction bands (43 ± 9°), when combined with the color analysis of the waveplate, leads us to conclude that the local optic axis of the LC was rotated counterclockwise during the application of the electric field (Figure 4a–d). We performed an experiment to confirm that rotation of the optic axis of the LC is not observed when an electric field is applied to a twisted LC sample (no NFF). We conclude that the rotation of the optic axis shown in Figure 4 arises from interactions of the NFF and LC (see also Supporting Information and Figure S7, Supporting Information).

We propose that the electro-optic response of an LC/NFF composite with a spiral pattern can be understood from the behavior of a single fiber (Figure 4e,f): without the field, the individual nanofibers (projected length of ≈10 μm on the *x*–*y* plane) are twisted when viewed from above due to their templated growth within the LC with a spiral configuration (Figure 4e). As the nanofibers are strained along the *z*-axis by the external electric field (Figure 4e), the projection of the nanofibers onto the *x*–*y* plane undergoes a counterclockwise rotation (Figure 4f). A similar mechanical behavior is also observed with a spring coil under axial loading, where the spring coil exhibits a decrease in radius perpendicular to its long axis above a threshold strain.[27,28] Since the nanofibers share their orientation with LC, the LC undergoes a counterclockwise reorientation on the *x*–*y* plane (Figure 4e).

We also characterized the optical response of the NFF/LC film upon the removal of the external field. When the external field was removed, the NFF/LC recovered its initial optical appearance, (Figure 4a,d), consistent with the relaxation of the NFF to its initial configuration. Overall, we conclude that the sharing of strain between the NFF and LC programs a complex yet reversible electrooptic responses of the composite.

3. Conclusion

The results in this paper demonstrate that LC-templated end-attached nanofibers grown by CVP are a promising route for fabricating soft nanocomposite materials that encode complex properties, including responses to external fields that appear promising for the design of new classes of electrooptic devices or soft actuators. Our mechanical modeling of the composite materials reveals that the mechanical response to external fields arises from a delicate balance of elastic and surface interactions, an insight that likely explains why prior studies of fibrous networks in LCs have not reported the reorganization of nanofiber networks in the manner described in our paper.[19] Specifically, our elastostatic model predicts that the mechanical coupling between nanofibers and LC is weakened substantially by a small increase in the fiber diameter or a decrease in the fiber length relative to that used in our experiments (average

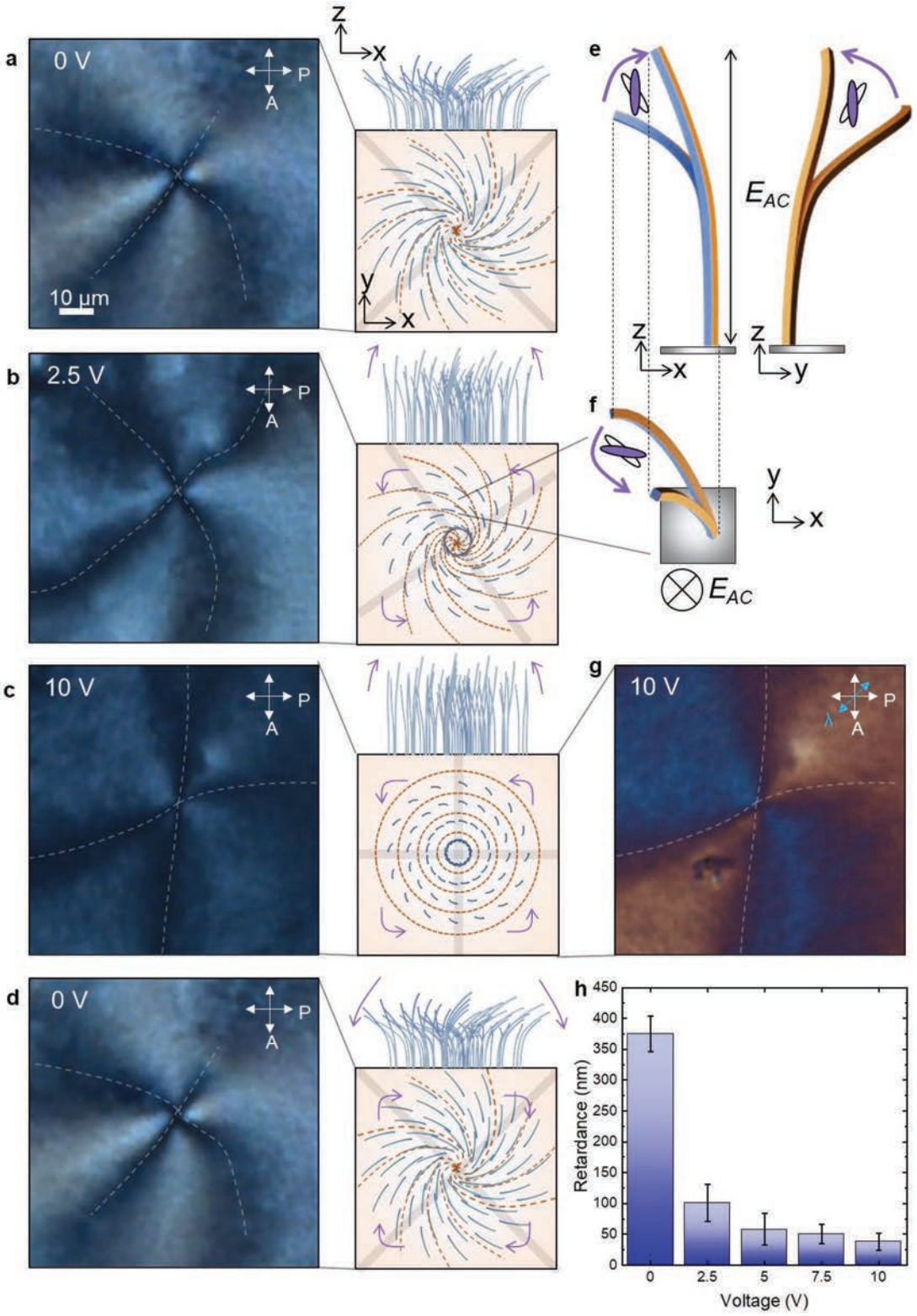

Figure 4. Changes in the optical appearance of an NFF-embedded LC under a) 0 V, b) 2.5 V, c) 10 V, and d) 0 V at 1 kHz (sine waveform, thickness ≈100 μm). A schematic illustration showing the side-view (bottom) and top-view (top) of the nanofiber organization is shown to the right of each optical micrograph. e,f) A schematic illustration of the deformation of a single nanofiber. g) The optical appearance of an NFF-embedded LC (10 V) with crossed polarizers and a wave plate (λ = 530 nm). The dotted lines indicate the rotation of extinction bands in (a–d) and (g). The direction of the polarizer, the analyzer, and the waveplate is indicated with the arrows. h) Change in the average retardance of LC (a–c) as a function of voltage. The error bars are 1 SD of retardance measured across the sample (a–c, n = 92 points each).

diameters of 74 ± 17 nm and lengths of 19 ± 4 μm). This result indicates that the nanofiber diameter and length must be precisely controlled to achieve efficient mechanical coupling to the LC (Figure S8, Supporting Information). This level of control is made possible by the use of CVP.[19]

While we focus on bent NFFs synthesized from achiral nematic LCs as an illustrative example in this study, the LC-templated CVP process is compatible with the use of cholesteric LCs or blue phase LC templates, thus allowing synthesis of a range of nanofiber shapes.[19] These various nanofiber shapes offer the potential to program distinct electromechanical and electrooptical responses into LC-nanofiber composites by virtue of the elastic energy stored in strained nanofibers. Such responses appear promising for the creation of advanced light valves and optical tweezers based on vortex light beams.[29,30] Finally, our results also reveal that CVP (Gorham reaction) can be combined with free radical polymerization to create polymer networks that encapsulate organized arrays of polymeric nanofibers. While fibers embedded in isotropic polymer networks have been shown to encode shape responses,[1,31,32] our results provide avenues for the synthesis of liquid crystalline networks (including elastomeric networks) with properties that are programmed by encapsulated arrays of nanofibers.[33–35]

4. Experimental Section

Chemical Vapor Polymerization: Synthesis of bent NFFs was carried out in a chemical vapor polymerization (CVP) system that consists of sublimation, pyrolysis, and deposition zones. In the deposition zone, TEM grids loaded with PCH LCs were placed on a rotating stage (10 rpm) to promote uniform polymerization of PCP-HM in the PCH LC. The PCH LC consists of 35 mol% of PCH3 (TCI) and 65 mol% of PCH5 (Sigma–Aldrich). To load PCH LC into a TEM grid, ≈0.2 μL of PCH LC was deposited using a micropipet into a copper TEM grid supported on a substrate and the excess amount of PCH LC was removed from the grid using a capillary tube. The PCP-HM was sublimed at a temperature of 120 °C in the sublimation zone and further pyrolyzed at 550 °C in the pyrolysis zone. A stream of argon gas flow was used to transport the sublimed and pyrolyzed PCP-HM to the deposition zone. The pressure of the deposition chamber was 0.1 mbar. The deposition rate of PCP-HM, which was read by a QCM sensor, was ≈0.02 nm s^{-1}. The entire deposition process was finished in ≈30 mins.

Microscopy: Figures 1d,e,h,i were taken using an optical microscope (Nikon Eclipse 80i) equipped with a digital camera (Sony CMOS Pregius sensor, DFK 23UX174). A white light source was used. The NFFs of Figure 1e,i were further rinsed with ethanol (Sigma–Aldrich) and acetone (Sigma–Aldrich) sequentially and agitated on an orbital shaker (KS 260 control, IKA). It was confirmed that this rinsing procedure enabled the preservation of the in-plane organization of nanofibers while LCs were thoroughly rinsed away. After drying the specimen, the NFFs in Figure 1f,g,j were further coated with Au and observed with a scanning electron microscope (SEM, FEG Tescan Mira3). The optical micrographs in Figures 2 and 4 were taken using an optical microscope (BX 41, Olympus) equipped with 4×, 10×, and 60× objectives, a Moticam 10.0 MP camera, and a halogen lamp (Philips 6 V 30 W bulb), two polarizers. The colors of the micrographs were calibrated with a white balance function in the digital camera software. Cryo-SEM (FEI Strata 400 STEM FIB) was used to visualize individual nanofibers embedded in the cross-linked LC (RM257/5CB mixture).The optical retardance was measured using both the Michel Levy interference color chart and PolScope (Polaviz, APSYS Inc.). Length and diameters of nanofibers were measured with the NFF-decorated surfaces after detaching the majority amount of nanofibers from substrates using sonication to visualize individual fibers.

Application of an Electric Field: ITO glasses (15 – 25 Ω sq^{-1}, Sigma–Aldrich) used as substrates were treated with H-PI (Nissan Chemical) after cleaning with ethanol. A function generator (Keysight, 33210A) connected to a voltage amplifier (Trek, ×500 V/V) was used to generate an electric field. A sine waveform at 1 kHz was used. Each side of the ITO glasses was attached with copper tapes (3M) and connected to the amplifier using alligator clips. For the optical cells with the thickness of ≈32 μm and ≈100 μm, glass beads (Cospheric LCC, d = 28–32 μm) and double-sided scotch tapes (3 M) were used, respectively.

Fabrication of Double Network LC Composites for Cryogenic SEM: A 30 w/v.% RM257 (BOC sciences) in 5CB (HCCH) was mixed on a hot stage (90 °C) with 0.1 wt.% of diphenyl (2,4,6-trimethyl benzoyl) phosphine oxide (TPO, Sigma–Aldrich) as a photoinitiator. After infusing the RM257 mixture into nanofiber cells, it was equilibrated for ≈30 mins on a 35 °C hot stage. Subsequently, the samples were cooled back to room temperature and cross-linked via UV light (365 nm) for ≈30 mins with/without applications of an electric field. The sample was detached from the substrates using a razor blade for cryogenic SEM analysis. A pristine glass substrate (Fisher) was used as a top layer for the sample prepared without an electric field.

Statistical Analysis: Error bars and sample sizes are defined in the legends of each figure. Numerical values of measured quantities are expressed as an average ± standard deviation (SD).

Supporting Information

Supporting Information is available from the Wiley Online Library or from the author.

Acknowledgements

S.R. and J.K. contributed equally to this work. The authors acknowledge NSF funding (CMMI-1916654) as a major source of funding for this study. The cryo-SEM work made use of the Cornell Center for Materials Research Shared Facilities which was supported through the NSF MRSEC program (DMR-1719875). Additional support for the FIB/SEM cryo-stage and transfer system was provided by the Kavli Institute at Cornell and the Energy Materials Center at Cornell (DE-SC0001086). The authors thank Katherine Anne Spoth for assisting with cryo-SEM sample preparation. The authors also thank Prof. Karthik Nayani for helpful suggestions throughout the study.

Conflict of Interest

The authors declare no conflict of interest.

Data Availability Statement

The data supporting the findings of this study are available within the article and its supplementary materials.

Keywords

chemical vapor polymerization, elastic strain, nanofibers forests, programmed response

[1] R. M. Erb, J. S. Sander, R. Grisch, A. R. Studart, *Nat. Commun.* **2013**, *4*, 1712.
[2] D. S. Fudge, N. Levy, S. Chiu, J. M. Gosline, *J. Exp. Biol.* **2005**, *208*, 4613.
[3] D. E. Ingber, D. Prusty, Z. Sun, H. Betensky, N. Wang, *J. Biomech.* **1995**, *28*, 1471.
[4] A. H. Williams, S. Roh, A. R. Jacob, S. D. Stoyanov, L. Hsiao, O. D. Velev, *Nat. Commun.* **2021**, *12*, 2834.
[5] I. Dierking, G. Scalia, P. Morales, *J. Appl. Phys.* **2005**, *97*, 044309.
[6] G. M. Koenig, I.-H. Lin, N. L. Abbott, *Proc. Natl. Acad. Sci. USA* **2010**, *107*, 3998.
[7] P. Poulin, H. Stark, T. C. Lubensky, D. A. Weitz, *Science* **1997**, *275*, 1770.
[8] P. C. Mushenheim, R. R. Trivedi, S. S. Roy, M. S. Arnold, D. B. Weibel, N. L. Abbott, *Soft Matter* **2015**, *11*, 6821.
[9] K. Nayani, A. A. Evans, S. E. Spagnolie, N. L. Abbott, *Proc. Natl. Acad. Sci. USA* **2020**, *117*, 26083.
[10] Y. Yuan, A. Martinez, B. Senyuk, M. Tasinkevych, I. I. Smalyukh, *Nat. Mater.* **2018**, *17*, 71.
[11] N. Mizoshita, Y. Suzuki, K. Hanabusa, T. Kato, *Adv. Mater.* **2005**, *17*, 692.
[12] R. Bao, C.-M. Liu, D. K. Yang, *Appl. Phys. Express* **2009**, *2*, 112401.
[13] D. Mănăilă-Maximean, O. Danila, C. P. Ganea, P. L. Almeida, *Eur. Phys. J. Plus* **2018**, *133*.
[14] P. G. de Gennes, J. Prost, *The Physics of Liquid Crystals*, Clarendon Press, **1993**.
[15] D. S. Miller, R. J. Carlton, P. C. Mushenheim, N. L. Abbott, *Langmuir* **2013**, *29*, 3154.
[16] M. Kleman, O. D. Lavrentovich, *Soft Matter Physics: An Introducion*, Springer, **2003**.
[17] C. Lapointe, A. Hultgren, D. M. Silevitch, E. J. Felton, D. H. Reich, R. L. Leheny, *Science* **2004**, *303*, 652.
[18] J. P. F. Lagerwall, G. Scalia, *J. Mater. Chem.* **2008**, *18*, 2890.
[19] K. C. K. Cheng, M. A. Bedolla-Pantoja, Y.-K. Kim, J. V. Gregory, F. Xie, A. De France, C. Hussal, K. Sun, N. L. Abbott, J. Lahann, *Science* **2018**, *362*, 804.
[20] M. M. de Luna, B. Chen, L. C. Bradley, R. Bhandia, M. Gupta, *J. Vac. Sci. Technol.* **2016**, *34*, 041403.
[21] K. Nayani, P. Rai, N. Bao, H. Yu, M. Mavrikakis, R. J. Twieg, N. L. Abbott, *Adv. Mater.* **2018**, *30*, 1706707.
[22] J. Li, S. Gauza, S.-T. Wu, *J. Appl. Phys.* **2004**, *96*, 19.
[23] M. A. Osman, Hp. Schad, H. R. Zeller, *J. Chem. Phys.* **1983**, *78*, 906.
[24] H. Y. Chen, J. Lahann, *Adv. Mater.* **2007**, *19*, 3801.
[25] S. Sen, K. Kali, S. K. Roy, S. B. Roy, *Mol. Cryst. Liq. Cryst.* **1985**, *126*, 269.
[26] X. Wang, E. Bukusoglu, D. S. Miller, M. A. Bedolla Pantoja, J. Xiang, O. D. Lavrentovich, N. L. Abbott, *Adv. Funct. Mater.* **2016**, *26*, 7343.
[27] X. Chen, S. Zhang, D. A. Dikin, W. Ding, R. S. Ruoff, L. Pan, Y. Nakayama, *Nano Lett.* **2003**, *3*, 1299.
[28] S. M. An, J. Ryu, M. Cho, K. J. Cho, *Smart Mater. Struct.* **2012**, *21*, 055009.
[29] E. Brasselet, N. Murazawa, H. Misawa, S. Juodkazis, *Phys. Rev. Lett.* **2009**, *103*, 103903.
[30] E. Brasselet, *Phys. Rev. Lett.* **2012**, *108*, 087901.
[31] A. Sydney Gladman, E. A. Matsumoto, R. G. Nuzzo, L. Mahadevan, J. A. Lewis, *Nat. Mater.* **2016**, *15*, 413.
[32] M. A. C. Stuart, W. T. S. Huck, J. Genzer, M. Müller, C. Ober, M. Stamm, G. B. Sukhorukov, I. Szleifer, V. V. Tsukruk, M. Urban, F. Winnik, S. Zauscher, I. Luzinov, S. Minko, *Nat. Mater.* **2010**, *9*, 101.
[33] F. Mondiot, X. Wang, J. J. de Pablo, N. L. Abbott, *J. Am. Chem. Soc.* **2013**, *135*, 9972.
[34] T. J. White, D. J. Broer, *Nat. Mater.* **2015**, *14*, 1087.
[35] T. H. Ware, M. E. McConney, J. J. Wie, V. P. Tondiglia, T. J. White, *Science* **2015**, *347*, 982.